

Two-dimensional $SU(N) \times SU(N)$ chiral models on the lattice

Paolo Rossi and Ettore Vicari

Dipartimento di Fisica dell'Università and I.N.F.N., I-56126 Pisa, Italy

(Received 7 September 1993)

Lattice $SU(N) \times SU(N)$ chiral models are analyzed by strong and weak coupling expansions and by numerical simulations. Twelfth-order strong coupling series for the free and internal energy are obtained for all $N \geq 6$. Three-loop contributions to the internal energy and to the lattice β function are evaluated for all N and nonuniversal corrections to the asymptotic Λ parameter are computed in the “temperature” and the “energy” schemes. Numerical simulations confirm a faster approach to asymptopia of the energy scheme. A phenomenological correlation between the peak in the specific heat and the dip of the β function is observed. Tests of scaling are performed for various physical quantities, finding substantial scaling at $\xi \gtrsim 2$. In particular, at $N = 6$ three different mass ratios are determined numerically and found in agreement, within statistical errors of about 1%, with the theoretical predictions from the exact S -matrix theory.

PACS number(s): 11.15.Ha, 11.15.Pg, 75.10.Hk

I. INTRODUCTION

Two-dimensional $SU(N) \times SU(N)$ principal chiral models defined by the continuum Lagrangian

$$L = \frac{1}{T} \text{Tr} \partial_\mu U \partial_\mu U^\dagger \quad (1)$$

are the simplest quantum field theories sharing with non-Abelian gauge theories the property of asymptotic freedom and whose large N limit is a sum over planar diagrams. Because of the existence of higher-order conservation laws, multiparticle amplitudes are factorized, and exact S matrices have been proposed [1–3]. The resulting bound state mass spectrum is represented by

$$M_r = M \frac{\sin(r\pi/N)}{\sin(\pi/N)}, \quad 1 \leq r \leq N-1, \quad (2)$$

and the bound state of r particles transforms as the totally antisymmetric tensor of rank r . The mass- Λ parameter ratio has been computed, and the result is [4]

$$\frac{M}{\Lambda_{\overline{\text{MS}}}} = \sqrt{\frac{8\pi}{e}} \frac{\sin \pi/N}{\pi/N}, \quad (3)$$

where $\overline{\text{MS}}$ denotes the modified minimal subtraction scheme. A “standard” lattice version of principal chiral models is obtained by choosing the action

$$S = -2\beta N \sum_{n,\mu} \text{Re} \text{Tr} [U_n U_{n+\mu}^\dagger], \quad \beta = \frac{1}{NT}, \quad (4)$$

whose properties have been investigated by several authors [5–11] especially by strong-coupling and mean field methods. Numerical simulations have also been per-

formed (at $N = 3$), most recently by Dagotto and Kogut [12] and Hasenbusch and Meyer [13].

As a preliminary step within a more general program whose ultimate goal is performing the numerical $1/N$ expansion of matrix-valued field theories, we decided to explore the properties of principal chiral models at larger-than-usual values of N . In particular we wanted to investigate the following issues: region of applicability, accuracy, and N dependence of the strong coupling series; the onset of scaling, with special attention to the interplay between thermodynamical (peak in the specific heat) and field theoretical (dip in the β -function) effects; a check of conjectured exact results (especially mass ratios) by Monte Carlo measurements in the scaling region; the role of coupling redefinitions in the widening of the asymptotic scaling regions.

To this purpose, we performed a variety of strong coupling and weak coupling calculations, and a number of numerical simulations for different values of N , and especially at $N = 6$, where the mass spectrum is sufficiently nontrivial (two independent mass ratios can be measured and compared with prediction), and $O(1/N^2)$ effects should be already significantly depressed.

In the present paper we only report on our analytical results, without offering any details on the derivations, that will be presented elsewhere.

II. ANALYTICAL RESULTS

A. Strong coupling

We found that the most convenient approach to strong coupling is the character expansion. Free energy character expansion for $U(N)$ chiral models to twelfth order and mass gap expansion to fifth order were presented in Ref. [5]. The formal extension of these series to $SU(N)$ is easily achieved with the above-mentioned precision for

$N > 6$. Paying some attention in order to avoid double-counting, $SU(6)$ can be also obtained by the same technique.

We found explicit representations of the coefficients of the $SU(N)$ character expansion in the strong coupling

regime in terms of Bessel functions, by generalizing the technique discussed in Refs. [11, 14]. These representations are exact up to $O(\beta^{2N})$. As a consequence we could compute the $SU(N)$ free energy to twelfth order in β for $N > 6$ in two dimensions:

$$\begin{aligned} \frac{1}{N^2}F &= 2\beta^2 + 2\beta^4 + 4\beta^6 + \left[14 + \frac{N^2(5N^2 - 2)}{(N^2 - 1)^2}\right]\beta^8 + \left[56 + \frac{8N^2(5N^2 - 2)}{(N^2 - 1)^2}\right]\beta^{10} \\ &+ \left[248 + \frac{8N^2(35N^2 - 17)}{(N^2 - 1)^2} + \frac{2N^2(14N^6 - 11N^4 + 8N^2 - 2)}{(N^2 - 1)^4} + \frac{16N^4(9N^4 - 26N^2 + 8)}{3(N^2 - 1)^2(N^2 - 4)^2}\right]\beta^{12} \\ &+ O(\beta^{14}) + 4\frac{N^{N-2}}{N!}\beta^N + \left[8\frac{N^{N-1}}{N!} - 4\frac{N^N}{(N+1)!}\right]\beta^{N+2} \\ &+ \left[2\frac{N^{N+2}}{(N+2)!} + 4\frac{N^{N+1}}{(N-1)N!} - 8\frac{(N+2)N^N}{(N+1)!} + 24\frac{N^{N-1}}{N!} + 4\frac{N^{N-2}}{(N-2)!}\right]\beta^{N+4} + O(\beta^{N+6}) . \end{aligned} \tag{5}$$

In the case $N = 6$ an analysis of the $O(\beta^{N+6})$ and $O(\beta^{2N})$ contributions led to the result

$$\begin{aligned} \frac{1}{N^2}F &= 2\beta^2 + 2\beta^4 + 11.2\beta^6 + 68.602449\beta^8 \\ &+ 374.945306\beta^{10} + 6395.760105\beta^{12} + \dots . \end{aligned} \tag{6}$$

The internal energy (per link) density E is immediately obtained from the previous results by

$$E = 1 - \frac{1}{4N^2} \frac{\partial F}{\partial \beta} . \tag{7}$$

These results have been used to draw the strong coupling curves in our figures and compare very well with numerical simulations in the region $\beta \lesssim 0.25$.

B. Weak coupling

Short weak coupling series for the free-energy density of $U(N)$ and $SU(N)$ chiral models were presented in Ref. [6].

We calculated the energy density up to three loops finding

$$\begin{aligned} E &= 1 - \left\langle \frac{1}{N} \text{Re Tr} [U_n U_{n+\mu}^\dagger] \right\rangle \\ &= \frac{N^2 - 1}{8N^2\beta} \left[1 + \frac{a_1}{\beta} + \frac{a_2}{\beta^2} + \dots \right] , \end{aligned} \tag{8}$$

where

$$\begin{aligned} a_1 &= \frac{N^2 - 2}{32N^2} , \\ a_2 &= \frac{3N^4 - 14N^2 + 20}{768N^4} + \frac{N^4 - 4N^2 + 12}{64N^4} Q_1 \\ &+ \frac{N^4 - 8N^2 + 24}{64N^4} Q_2 , \end{aligned} \tag{9}$$

Q_1 and Q_2 being numerical constants: $Q_1 = 0.0958876$

and $Q_2 = -0.0670$.

Asymptotic scaling requires the ratio of any dimensional quantity to the appropriate power of the two-loop lattice scale ,

$$\Lambda_{L,2l} = (b_0 T)^{-b_1/b_0^2} \exp\left(-\frac{1}{b_0 T}\right) , \tag{10}$$

to go to a constant as $T \rightarrow 0$. b_0 and b_1 are the first universal coefficients of the expansion of the β function:

$$\beta_L(T) \equiv -a \frac{d}{da} T = -b_0 T^2 - b_1 T^3 - b_{2L} T^4 + \dots , \tag{11}$$

$$b_0 = \frac{N}{8\pi} , \quad b_1 = \frac{N^2}{128\pi^2} . \tag{12}$$

Evaluation of the ratios of Λ parameters requires a one-loop calculation in perturbation theory, which leads to [8]

$$\frac{\Lambda_{MS}}{\Lambda_L} = \sqrt{32} \exp\left(\pi \frac{N^2 - 2}{2N^2}\right) . \tag{13}$$

In order to get a more accurate description of the approach to asymptotic scaling we performed the change of variables suggested by Parisi [15], defining a new temperature T_E proportional to the energy:

$$T_E = \frac{8N}{N^2 - 1} E , \quad \beta_E = \frac{1}{NT_E} . \tag{14}$$

Notice that the corresponding specific heat is, by definition, constant. The ratio of Λ_E , the Λ parameter of the β_E scheme, and Λ_L is easily obtained from the two-loop term of the energy density:

$$\frac{\Lambda_E}{\Lambda_L} = \exp\left(\pi \frac{N^2 - 2}{4N^2}\right) . \tag{15}$$

We encountered the usual (and yet unexplained) phe-

nomenon of a much better convergence to asymptotic scaling for quantities plotted as functions of β_E [16–18]. We tried to check for a perturbative explanation of this phenomenon by computing the first perturbative correction to the two loop lattice scale,

$$\Lambda = (8\pi\beta)^{1/2} e^{-8\pi\beta} \left[1 + \frac{b_1^2 - b_0 b_2}{N b_0^3} \beta^{-1} + O(\beta^{-2}) \right], \quad (16)$$

in the standard and the β_E scheme, which requires the calculation of the three-loop term of the β function in both schemes.

In the standard scheme we found

$$b_{2L} = \frac{1}{(2\pi)^3} \frac{N^3}{128} \left[1 + \pi \frac{N^2 - 2}{2N^2} - \pi^2 \left(\frac{2N^4 - 13N^2 + 18}{6N^4} + 4G_1 \right) \right], \quad (17)$$

where $G_1 = 0.04616363$ [19, 20]. The equivalence of the $SU(2) \times SU(2)$ chiral model to the $O(4)$ σ model allows a check of this equation; indeed for $N = 2$ it must give (and indeed it does) the same b_{2L} of the standard lattice $O(4)$ σ model [19].

The β function of the β_E scheme can be written in the form

$$\beta_E(T_E) \equiv -a \frac{d}{da} T_E = \frac{8N^2}{N^2 - 1} C(T) \beta_L(T), \quad (18)$$

where

$$C(T) \equiv \frac{1}{N} \frac{dE}{dT} \quad (19)$$

is the specific heat and T must be considered as a function of T_E . Expanding perturbatively Eq. (18) and using Eq. (8) one finds

$$b_{2E} = b_{2L} + N^2 b_0 (a_2 - a_1^2) + N b_1 a_1. \quad (20)$$

As one may easily verify, the linear corrections to the two-loop lattice scale in Eq. (16) are small and of the same order of magnitude (although of opposite sign). They cannot therefore explain the failure of the first and the success of the second scheme with respect to achieving asymptotic scaling. We believe that the origin of this

phenomenon is fully nonperturbative, and it can presumably be traced to the phenomenologically apparent correlation existing between the peak in the specific heat and the dip in the lattice β function: the nonperturbative variable transformation that flattens the peak manages to fill the dip, in a theoretically yet uncontrolled way.

III. NUMERICAL RESULTS

We performed Monte Carlo simulations of the lattice $SU(N) \times SU(N)$ chiral models for a wide range of values of N (in particular $N = 3, 6, 9, 15$) and β . Summaries of the runs are presented in Tables I, II, III, and IV.

In our simulations we implemented the Cabibbo-Marinari algorithm [21] to upgrade $SU(N)$ matrices by updating its $SU(2)$ subgroups. In most cases, we chose to update the $N - 1$ diagonal subsequent $SU(2)$ subgroups of each $SU(N)$ matrix variable by employing the overheat-bath algorithm [22] (for the “heat bath” part of it we used the Kennedy-Pendleton algorithm [23]).

An important class of observables of the $SU(N) \times SU(N)$ chiral models can be constructed by considering the group invariant correlation function

$$G(x - y) = \left\langle \frac{1}{N} \text{Re Tr} [U(x)U(y)^\dagger] \right\rangle. \quad (21)$$

We define the correlation function ξ_G from the second moment of the correlation function $G(x)$. On the lattice

$$\xi_G^2 = \frac{1}{4 \sin^2 \pi/L} \left[\frac{\tilde{G}(0,0)}{\tilde{G}(0,1)} - 1 \right], \quad (22)$$

where $\tilde{G}(k_x, k_y)$ is the Fourier transform of $G(x)$. The inverse mass gap ξ_w is extracted from the long distance behavior of the zero space momentum correlation function constructed with $G(x)$. Moreover we measured the diagonal wall-wall correlation length ξ_d to test rotation invariance. $M \equiv 1/\xi_w$ should reproduce in the continuum limit the mass of the fundamental state. The first definition of correlation length ξ_G offers the advantage of being directly measurable, while the calculation of ξ_w requires a fit procedure. On the other hand, since ξ_G is an off-shell quantity an analytical prediction exists only for the inverse mass-gap [Eq. (3)].

In Tables I, II, III, and IV we present data for the energy density E , the specific heat $C \equiv \frac{1}{N} \frac{dE}{dT}$, the magnetic

TABLE I. Summary of the numerical results for $N = 3$.

β	L	E	C	χ_m	ξ_G	ξ_G/ξ_w	ξ_d/ξ_w
0.18	18	0.74118(5)	0.0712(4)	3.843(5)	1.003(17)		
0.225	24	0.62819(12)	0.143(2)	9.15(3)	1.87(2)	0.990(10)	0.994(13)
0.25	30	0.55589(4)	0.1814(9)	19.09(4)	3.027(14)	0.986(5)	0.995(7)
0.27	36	0.49992(4)	0.1935(10)	40.22(9)	4.79(2)	0.988(3)	1.004(4)
0.27	42	0.50000(3)	0.1936(10)	40.05(9)	4.78(2)	0.987(5)	0.999(3)
0.27	48	0.50003(3)	0.1918(12)	40.21(9)	4.81(3)	0.984(6)	0.995(6)
0.29	81	0.45172(3)	0.187(2)	93.1(5)	7.99(10)	0.989(10)	1.000(10)
0.30	90	0.43111(2)	0.176(2)	144.2(8)	10.41(10)	0.993(7)	0.989(9)
0.315	120	0.40400(2)	0.166(3)	283(3)	15.5(3)	0.981(9)	0.997(12)

TABLE II. Summary of the numerical results for $N = 6$.

β	L	E	C	χ_m	ξ_G	ξ_G/ξ_w	ξ_d/ξ_w
0.10	15	0.89781(3)	0.01076(7)	1.5717(12)	0.396(12)		
0.15	18	0.84170(2)	0.02690(10)	2.091(2)	0.56(2)		
0.175	18	0.81060(2)	0.0399(2)	2.4806(14)	0.671(9)		
0.20	24	0.77592(2)	0.0596(3)	3.0425(18)	0.816(12)		
0.225	18	0.73506(4)	0.0903(6)	3.936(3)			
0.25	18	0.68234(8)	0.153(2)	5.731(9)	1.332(10)	0.987(11)	0.998(15)
0.26	24	0.65537(7)	0.200(3)	7.120(11)	1.560(14)		
0.27	24	0.62377(5)	0.248(2)	9.407(9)	1.882(6)	0.991(7)	0.998(7)
0.28	30	0.58690(8)	0.302(4)	13.68(3)	2.410(17)	0.994(6)	0.997(6)
0.285	30	0.56710(7)	0.332(6)	17.28(3)	2.836(13)	0.989(6)	1.007(7)
0.29	30	0.54730(7)	0.323(4)	22.31(5)	3.354(18)	0.991(8)	0.992(5)
0.29	36	0.54732(7)	0.323(5)	22.38(6)	3.37(2)	0.986(6)	0.996(8)
0.30	36	0.51134(5)	0.300(4)	38.27(9)	4.75(2)	0.989(4)	0.996(4)
0.30	42	0.51134(5)	0.296(3)	38.30(12)	4.76(2)	0.994(6)	0.998(10)
0.30	48	0.51139(8)	0.288(8)	38.23(16)	4.78(5)	0.999(6)	0.995(5)
0.31	54	0.48188(4)	0.256(3)	65.1(3)	6.55(5)	0.986(6)	1.005(5)
0.31	60	0.48186(4)	0.258(4)	65.1(2)	6.61(4)	0.992(5)	1.000(7)
0.32	75	0.45764(3)	0.227(3)	108.4(5)	9.14(7)	0.996(5)	0.995(7)
0.32	81	0.45769(3)	0.230(5)	107.4(6)	9.00(11)	0.997(7)	1.001(8)
0.40	60	0.34033(5)					
0.50	60	0.26335(4)					

TABLE III. Summary of the numerical results for $N = 9$.

β	L	E	C	χ_m	ξ_G	ξ_G/ξ_w	ξ_d/ξ_w
0.175	18	0.812908(11)	0.03769(13)	2.4494(12)	0.672(7)		
0.20	24	0.780870(12)	0.0538(3)	2.948(12)	0.792(10)		
0.25	18	0.70339(8)	0.120(2)	4.868(8)	1.177(11)		
0.27	24	0.65937(13)	0.205(6)	6.792(15)	1.497(17)	0.980(8)	0.995(10)
0.28	24	0.62920(12)	0.268(8)	8.78(2)	1.777(13)	0.990(9)	0.997(10)
0.29	30	0.58801(13)	0.410(15)	13.27(3)	2.371(14)	0.994(7)	0.987(7)
0.295	36	0.56281(12)	0.457(16)	17.96(5)	2.89(2)	0.994(7)	0.998(5)
0.30	30	0.53844(21)	0.420(25)	25.36(14)	3.67(3)		
0.30	36	0.53845(16)	0.411(21)	25.22(12)	3.63(4)	0.992(8)	0.998(8)
0.30	42	0.53847(12)	0.411(16)	25.26(9)	3.68(4)	0.999(6)	1.009(6)
0.31	42	0.50028(9)	0.307(12)	47.1(2)	5.39(5)		
0.31	54	0.50035(9)	0.318(12)	47.2(2)	5.46(5)	0.993(9)	0.995(10)
0.32	60	0.47234(5)	0.252(10)	81.6(4)	7.65(7)	0.995(4)	1.006(5)

TABLE IV. Summary of the numerical results for $N = 15$.

β	L	E	C	χ_m	ξ_G	ξ_G/ξ_w	ξ_d/ξ_w
0.20	24	0.781395(16)	0.0515(5)	2.9392(14)	0.775(12)		
0.25	24	0.70846(3)	0.100(3)	4.692(4)	1.158(14)		
0.28	24	0.64990(9)	0.204(8)	7.251(11)	1.561(10)	0.997(10)	0.992(9)
0.29	24	0.62134(13)	0.294(14)	9.31(2)	1.857(9)	0.998(6)	0.995(7)
0.30	30	0.56809(18)	0.67(4)	16.53(5)	2.750(12)	0.995(5)	1.000(6)
0.31	45	0.51202(10)	0.35(3)	38.89(16)	4.78(3)	0.983(8)	0.998(7)

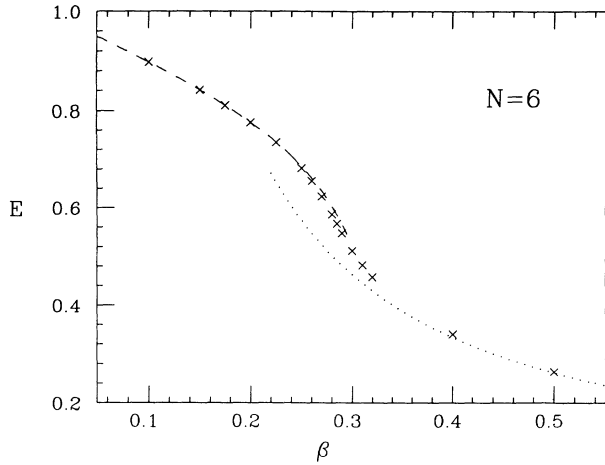


FIG. 1. Energy versus β for $N = 6$. The dashed and dotted lines represent respectively the 12th order strong coupling and the third-order weak coupling series.

susceptibility χ_m defined from the correlation function $G(x)$, the correlation length ξ_G , and the dimensionless ratios ξ_G/ξ_w and ξ_d/ξ_w , respectively, for $N = 3, 6, 9, 15$.

We carefully checked for finite size effects. It turned out that for $z \equiv L/\xi_G \gtrsim 8$ the finite size systematic errors in evaluating infinite volume quantities should be safely smaller than 1%, which is the typical statistical error of our data.

In Figs. 1 and 2 we show the energy density versus β respectively at $N = 6$ and $N = 9$. There the strong coupling series up to twelfth order in β and the weak coupling one up to third order in β^{-1} are drawn.

As in other asymptotically free models, at all values of N the specific heat shows a peak, connecting the two different asymptotic behaviors, monotonically increasing in the strong coupling region and decreasing at large β . In Figs. 3, 4, 5, and 6 C is plotted respectively for $N = 3, 6, 9, 15$ with the corresponding 13th order strong coupling series (except for $N = 3$). Increasing

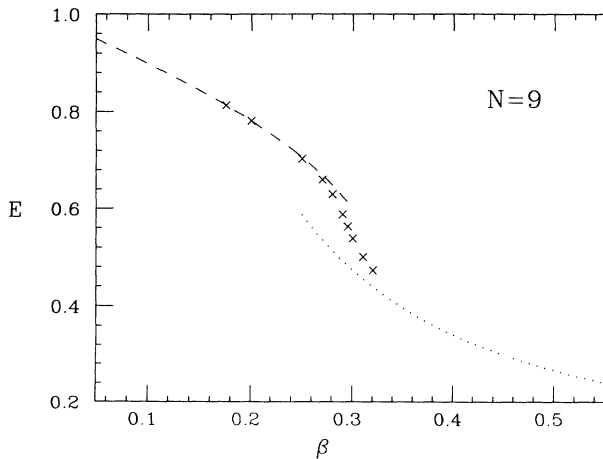


FIG. 2. Energy versus β for $N = 9$. The dashed and dotted lines represent respectively the 12th-order strong coupling and the third-order weak coupling series.

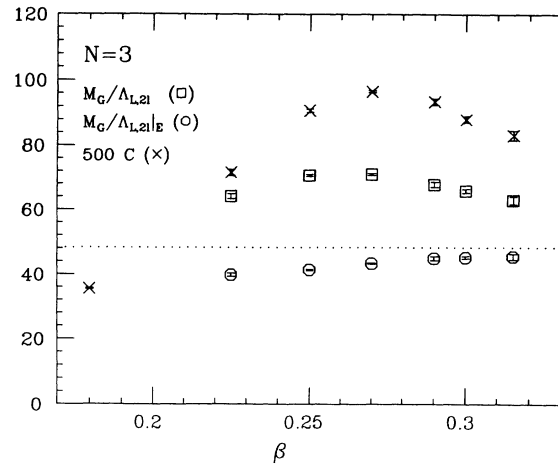


FIG. 3. Specific heat and asymptotic scaling test $M_G/\Lambda_{L,2l}$ for $N = 3$. The dashed line shows the analytical prediction (3). Data of C are multiplied by 500.

ing N , the peak moves slightly towards higher β values ($\beta_{\text{peak}} \simeq 0.285$ at $N = 6$, $\beta_{\text{peak}} \simeq 0.30$ at $N = 15$), and becomes more and more pronounced. We found the position of the peak to be more stable at large N when plotting C versus ξ_G , as in Fig. 7. Notice that, increasing N , the specific heat around the peak does not show any apparent convergence to a finite value, which might be an indication of a (first order?) phase transition at $N = \infty$.

The 12th order (13th order) strong coupling series of the energy (specific heat) are in quantitative agreement (within our statistical errors) for $\beta \lesssim 0.2$, and in qualitative agreement up to the peak of the specific heat, whose position should give an estimate of the strong coupling convergence radius.

Tests of scaling, based on the stability of dimensionless

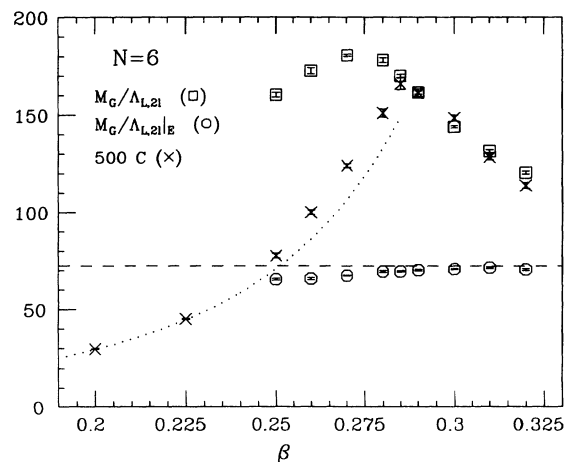


FIG. 4. Specific heat and asymptotic scaling test $M_G/\Lambda_{L,2l}$ for $N = 6$. The dotted line represents the 13th-order strong coupling series of C . The dashed line shows the analytical prediction (3). Data of C and the corresponding strong coupling series are multiplied by 500.

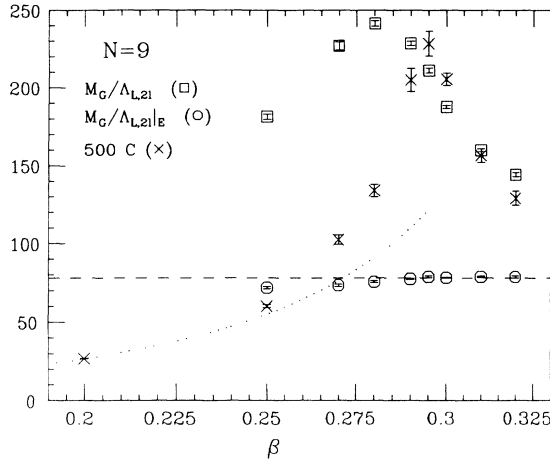


FIG. 5. Specific heat and asymptotic scaling test $M_G/\Lambda_{L,2l}$ for $N = 9$. The dotted line represents the 13th-order strong coupling series of C . The dashed line shows the analytical prediction (3).

physical quantities (for example, the ratio ξ_G/ξ_w) and rotation invariance (checking that $\xi_w/\xi_d \simeq 1$), showed that, within our statistical errors, the scaling region is reached already at small correlation lengths, i.e., for $\xi_G \simeq 2$. Fitting data in the scaling region to a constant we found

$$\begin{aligned} \xi_G/\xi_w &= 0.987(2) \quad \text{for } N = 3 \\ &= 0.993(2) \quad \text{for } N = 6 \\ &= 0.995(3) \quad \text{for } N = 9 \\ &= 0.994(4) \quad \text{for } N = 15 \end{aligned} \quad (23)$$

Notice that scaling is observed even before the peak of the specific heat. Since strong coupling series should be effective in this region, it might be possible to calculate continuum physical quantities by strong coupling techniques. In order to investigate this issue, work to extend

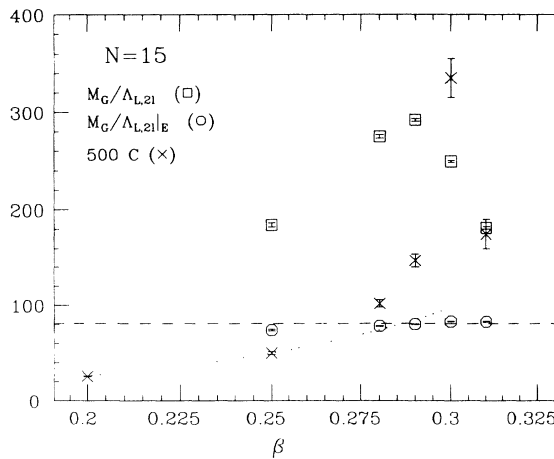


FIG. 6. Specific heat and asymptotic scaling test $M_G/\Lambda_{L,2l}$ for $N = 15$. The dotted line represents the 13th-order strong coupling series of C . The dashed line shows the analytical prediction (3).

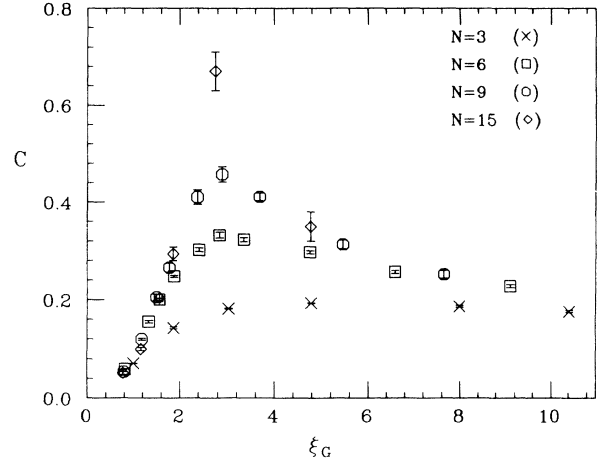


FIG. 7. Specific heat versus ξ_G .

the strong coupling series is in progress.

We checked asymptotic scaling according to the two-loop formula (10) by analyzing $M_G/\Lambda_{L,2l} \equiv 1/(\xi_G \Lambda_{L,2l})$. In Figs. 3, 4, 5, and 6 we show the corresponding data respectively for $N = 3, 6, 9$, and 15. At all values of N we observe the usual dip in the β function, which is, again, more and more pronounced when increasing N . Since $\xi_G \simeq \xi_w$ we compare $M_G/\Lambda_{L,2l}$ directly with Eq. (3) [using also Eq. (13)], whose predictions,

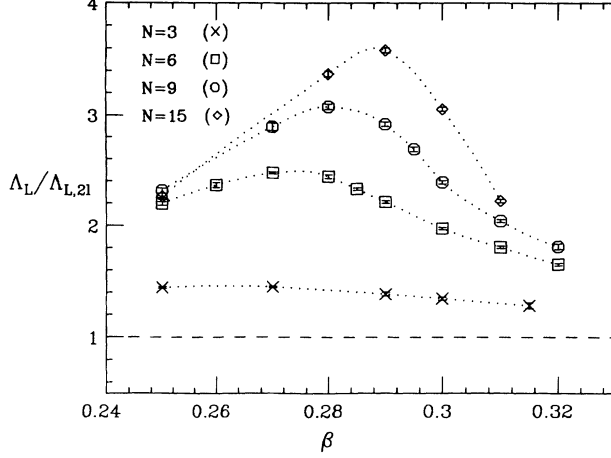
$$\begin{aligned} M/\Lambda_L &= 48.266\dots \quad \text{for } N = 3 \\ &= 72.412\dots \quad \text{for } N = 6 \\ &= 77.989\dots \quad \text{for } N = 9 \\ &= 81.001\dots \quad \text{for } N = 15 \end{aligned} \quad (24)$$

are represented by dashed lines in the figures. Notice that the Monte Carlo data are much larger than the predicted values, while the first perturbative corrections in Eq. (16) are, in all cases, about 20% at $\beta \simeq 0.3$. Furthermore, data show a similarity with the behavior of the specific heat, strengthening the idea of a strong correlation between the two phenomena.

The approach to asymptotic scaling gets an impressive improvement using the β_E scheme. In Figs. 3, 4, 5, and 6 we also plot

$$M_G/\Lambda_{L,2l|E} \equiv \frac{1}{\xi_G \Lambda_{E,2l}} \frac{\Lambda_E}{\Lambda_L} \quad (25)$$

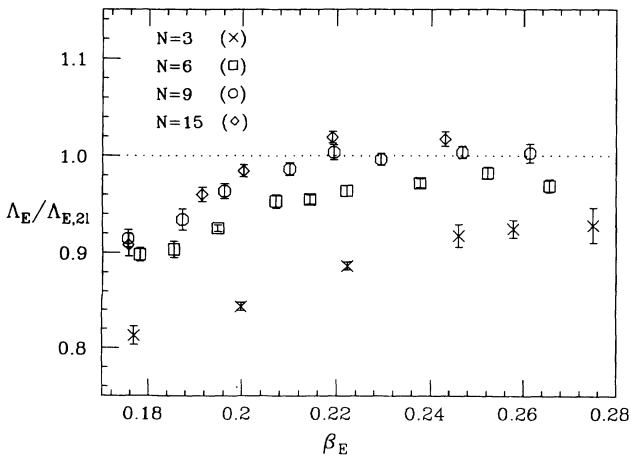
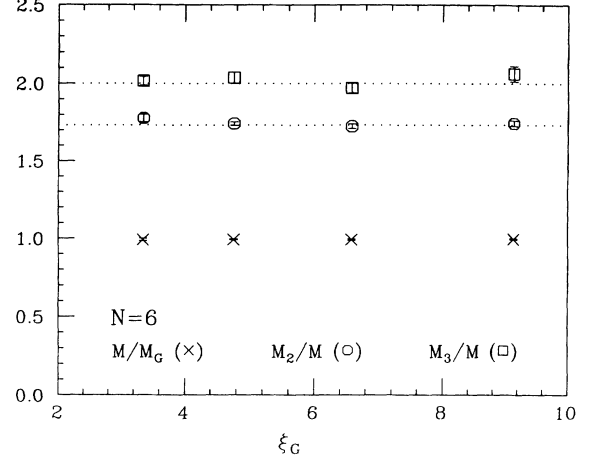
Now data approach the correct value, and the discrepancies are even smaller than the linear correction calculated in Sec. III (which is about 15% at $\beta \simeq 0.3$). So flattening the peak of the specific heat by performing the coupling redefinitions $T \rightarrow T_E$, the dip of the β function disappears. We believe this to be the key point of the success of the β_E scheme in widening the asymptotic scaling region. The peak of the specific heat should be explicable in terms of complex β singularities of the partition function close to the real axis [24]. The sharpening of the peak with increasing N would indicate that the complex singularities get nearer and nearer to the real axis, pinching it at $N = \infty$ where a phase transition is

FIG. 8. $\Lambda_L(N, \beta) / \Lambda_{L,2l}(N, \beta)$ versus β .

expected. Such singularities should also cause the abrupt departure from the weak coupling behavior. Then a coupling transformation eliminating the peak should move the complex β -singularities away from the real axis, and therefore improve the approach to asymptotic scaling.

From the Monte Carlo data and the exact result (3) we can extract the effective Λ parameters $\Lambda_L(N, \beta)$ and $\Lambda_E(N, \beta_E)$. Figures 8 and 9 show respectively the ratios $\Lambda_L(N, \beta) / \Lambda_{L,2l}(N, \beta)$ and $\Lambda_E(N, \beta_E) / \Lambda_{E,2l}(N, \beta_E)$, where $\Lambda_{L,2l}(N, \beta)$ and $\Lambda_{E,2l}(N, \beta_E)$ are the corresponding two-loop functions: $\Lambda_{L,2l}(N, x) = \Lambda_{E,2l}(N, x) = (8\pi x)^{1/2} \exp(-8\pi x)$. Similarly to the specific heat, the effective Λ parameter $\Lambda_L(N, \beta)$ does not give evidence of convergence at large N . On the contrary $\Lambda_E(N, \beta_E)$ appears to approach a finite function $\Lambda_E(\infty, \beta_E)$, which is well approximated by the two-loop formula.

In conclusion, scaling and asymptotic scaling (in the β_E scheme) are observed at all values of N considered, even around the peak of the specific heat. It is interesting to notice that, even though the behavior of the specific heat with respect to N suggests the existence of a phase transition at $N = \infty$, the above scenario is apparently stable at large N .

FIG. 9. $\Lambda_E(N, \beta_E) / \Lambda_{E,2l}(N, \beta_E)$ versus β_E .FIG. 10. M/M_G , M_2/M , and M_3/M versus ξ_G for $N = 6$. Dotted lines show the exact predictions (2) for the ratios M_2/M and M_3/M .

IV. MASS SPECTRUM AT $N = 6$

We studied the mass spectrum at $N = 6$, where Eq. (2) predicts the existence of two independent mass ratios. In order to extract the other two independent mass values besides the fundamental one, we considered the operators

$$O_{abcd}^{(2)} = U_{ab}U_{cd} - U_{ad}U_{cb} \quad , \quad (26)$$

$$O_{abcdef}^{(3)} = U_{ab}U_{cd}U_{ef} - U_{ab}U_{cf}U_{ed} - U_{ad}U_{cb}U_{ef} \\ + U_{ad}U_{cf}U_{eb} + U_{af}U_{cb}U_{ed} - U_{af}U_{cd}U_{eb} \quad (27)$$

having respectively the same transformation properties of the two and three particle bound states. The mass values M_2 and M_3 were determined from the large distance behavior of the zero space momentum correlation functions constructed with the above operators. In practice we found distances $d \gtrsim 1.5\xi_G$ to be large enough to fit the data to the expected exponential behavior. In Table V and in Fig. 10 we present the data for the ratios M/M_G , M_2/M , and M_3/M , analyzed using the jackknife method. They show good scaling. Fitting them to a constant we found

TABLE V. Mass spectrum for $N = 6$.

β	M/M_G	M_2/M	M_3/M
0.29	0.991(8)	1.78(3)	2.02(3)
0.30	0.993(3)	1.74(2)	2.04(4)
0.31	0.992(4)	1.72(2)	1.98(3)
0.32	0.996(4)	1.74(2)	2.06(5)

$$\begin{aligned}
 M/M_G &= 0.993(2) \quad , \\
 M_2/M &= 1.74(1) \quad , \\
 M_3/M &= 2.01(2) \quad .
 \end{aligned}
 \tag{28}$$

This result confirms, within statistical errors of about

1%, the conjectured exact result (2), which predicts

$$\begin{aligned}
 M_2/M &= 1.73205\dots \quad , \\
 M_3/M &= 2 \quad .
 \end{aligned}
 \tag{29}$$

-
- [1] E. Abdalla, M.C.B. Abdalla, and A. Lima-Santos, Phys. Lett. **140B**, 71 (1984).
- [2] P. Wiegmann, Phys. Lett. **141B**, 217 (1984).
- [3] P. Wiegmann, Phys. Lett. **142B**, 173 (1984).
- [4] J. Balog, S. Naik, F. Niedermayer, and P. Weisz, Phys. Rev. Lett. **69**, 873 (1992).
- [5] F. Green and S. Samuel, Nucl. Phys. **B190**, 113 (1981).
- [6] Y. Brihaye and P. Rossi, Nucl. Phys. **B235**, 226 (1984).
- [7] J. Shigemitsu, J.B. Kogut, and D.K. Sinclair, Phys. Lett. **100B**, 316 (1981).
- [8] J. Shigemitsu and J.B. Kogut, Nucl. Phys. **B190**, 365 (1981).
- [9] J. Kogut, M. Snow, and M. Stone, Phys. Rev. Lett. **47**, 1767 (1981).
- [10] J. Kogut, M. Snow, and M. Stone, Nucl. Phys. **B215**, 45 (1983).
- [11] A. Guha and S.C. Lee, Nucl. Phys. **B240**, 141 (1984).
- [12] F. Dagotto and J.B. Kogut, Nucl. Phys. **B290**, 451 (1987).
- [13] M. Hasenbusch and S. Meyer, Phys. Rev. Lett. **68**, 435 (1992).
- [14] P. Rossi, Phys. Lett. **117B**, 72 (1982).
- [15] G. Parisi, in *High Energy Physics—1980*, Proceedings of the XXth International Conference on High Energy Physics, Madison, Wisconsin, 1980, edited by L. Durand and L. G. Pondrom, AIP Conf. Proc. No. 68 (AIP, New York, 1981).
- [16] F. Karsch and R. Petronzio, Phys. Lett. **139B**, 403 (1984).
- [17] U. Wolff, Phys. Lett. B **248**, 335 (1990).
- [18] M. Campostrini, P. Rossi, and E. Vicari, Phys. Rev. D **43**, 4643 (1992).
- [19] M. Falcioni and A. Treves, Nucl. Phys. **B265**, 671 (1986).
- [20] M. Campostrini and P. Rossi, Phys. Lett. B **242**, 225 (1990).
- [21] N. Cabibbo and E. Marinari, Phys. Lett. **119B**, 387 (1982).
- [22] R. Petronzio and E. Vicari, Phys. Lett. B **254**, 444 (1991).
- [23] A.D. Kennedy and B.J. Pendleton, Phys. Lett. **156B**, 393 (1985).
- [24] M. Falcioni, E. Marinari, M.L. Paciello, G. Parisi, and B. Taglienti, Phys. Lett. **102B**, 270 (1981); **108B**, 331 (1982).